ISPRS Journal of Photogrammetry and Remote Sensing 92 (2014) 16–25

Contents lists available at ScienceDirect

ISPRS Journal of Photogrammetry and Remote Sensing

journal homepage: www.elsevier.com/locate/isprsjprs

A first in-flight absolute calibration of the Chilean Earth Observation Satellite

C. Mattar [a], J. Hernández [b], A. Santamaría-Artigas [a,*], C. Durán-Alarcón [a], L. Olivera-Guerra [a], M. Inzunza [c], D. Tapia [c], E. Escobar-lavín [c]

[a] Laboratory for Analysis of the Biosphere (LAB), Dpt. of Environmental Sciences and Renewable Natural Resources, University of Chile, Av. Santa Rosa 11315, La Pintana, Santiago, Chile
[b] Geomatics and Landscape Ecology Lab, Forestry and Nature Conservation Faculty, University of Chile, Av. Santa Rosa 11315, La Pintana, Santiago, Chile
[c] Spatial Operation Group, Chilean Air Force, Volcán Osorno s/n, El Bosque, Santiago, Chile

ARTICLE INFO

Article history:
Received 9 August 2013
Received in revised form 21 January 2014
Accepted 26 February 2014
Available online 26 March 2014

Keywords:
Radiometric calibration
Reflectance
Fasat-C
Atmospheric correction
Aerosol
6S
MODIS

ABSTRACT

This work describes the first in-flight absolute calibration of the "*Sistema Satelital para la Observación de la Tierra*" (SSOT or Fasat-C). It was performed on January 29th 2013 at Antumapu site located in the southern area of Santiago, Chile. A description of the procedure is presented which includes both ground measurement and atmospheric characterization. The Chilean satellite for Earth observation carries on board a "New AstroSat Optical Modular Instrument" (NAOMI) high-resolution pushbroom imager which provides a 1.45 m ground sampling distance in the panchromatic (0.455–0.744 μm) channel and a 5.8 m ground sampling distance for the green (0.455–0.52 μm), blue (0.528–0.588 μm), red (0.625–0.695 μm) and near-infrared (0.758–0.881 μm) channels from a 620 km orbit. Radiometric calibration was carried out in order to estimate the land leaving radiance and bidirectional reflectance at the top of the atmosphere. To correct the reflectance data for atmospheric effects, the Second Simulation of a Satellite Signal in the Solar Spectrum (6S) code was used. Aerosol Optical Depth (AOD), water vapor and ozone content were obtained from MOD04, MOD05 and MOD07 products respectively, which are derived from the Moderate Resolution Imaging Spectroradiometer (MODIS) data. Statistical results such as BIAS, SIGMA and RMSE were calculated for the comparison between surface reflectance values and in situ measurements. Results show that the overall accuracy of the atmospherically corrected surface reflectance calculated from Fasat-C imagery can be estimated to around ±5%, with a R^2 coefficient of 0.939 between atmospherically corrected reflectance values and in situ measurements. The atmospheric correction applied in this work by combining MODIS data and the 6S radiative transfer code could be used for further calibration of the Fasat-C images, although in situ atmospheric irradiance measurements are necessary to estimate reliable values of surface reflectance. Future validation tasks have been considered for further applications to natural resources management and surface land cover classification.

1. Introduction

The SSOT (Sistema Satelital para la Observación de la Tierra; referred hereafter as Fasat-C) was launched on December 16th, 2011, becoming the first successful Chilean satellite mission. One of the main purposes of the Fasat-C is the ability to detect and quantify changes in the Chilean territory, to generate the bases for fast emergency response in the case of earthquakes or volcanic eruptions and to monitor the natural surfaces affected by climate change (i.e. glaciers or southern dense forests), among other environmental applications.

Fasat-C imagery is useful to obtain biophysical parameters from the land surface covers. These images can be used in several applications such as environmental monitoring, mining activities, agricultural production and natural resource management, among others. Both temporal and spatial resolution can contribute to develop more efficient productive process on the Chilean productivity system by considering Fasat-C images in order to fill the gaps between technological developments and productive systems.

However, consistent measurements on the Earth's surface have to be calibrated (to both known accuracy and precision) in order to provide reliable scientific information to discriminate between artifacts and changes in the Earth process which are being monitored (Roy et al., 2002). Thus, a radiometric characterization and

* Corresponding author.
E-mail address: andres.santamaria.artigas@gmail.com (A. Santamaría-Artigas).

http://dx.doi.org/10.1016/j.isprsjprs.2014.02.017
0924-2716/

calibration is an essential prerequisite for creating high-quality science data, and consequently, higher level downstream products (Chander et al., 2009).

The success of any remote sensing program depends upon the knowledge of both the spectral and radiometric characteristics of the sensor from which the data will be available (Thome et al., 2004). Since the launch of the Fasat-C, users have asked for technical information and radiometric calibration of the different level products generated by the Chilean Aerospace Operation Group (GOE). Therefore, the basic data allowing the conversion of the digital numbers to physical data are a current need that has to be fulfilled. Because there was no reliable pre-launch data or simulation, it was necessary to carry out an in-flight absolute calibration of the Fasat-C data. The main objective of this work is to presents the basic steps necessary in order to carry out a consistent radiometric calibration of the Fasat-C Level 2 products in order to convert the digital number to at-sensor (or apparent) reflectance, and in addition to present the first absolute in-flight calibration. Moreover, a reflectance-based method is described to present the relative errors achieved by comparing the surface reflectance estimated by the Fasat-C with in situ ground measurements. This work is structured as follows: Section 2 presents an overview of the Fasat-C such as technical features, spectral bands, calibration coefficients and solar irradiance values. Section 3 describes the study area and the data acquisition for the radiometric calibration. Section 4 presents the method used for the radiometric calibration of Fasat-C data. Section 5 shows the results obtained for the in-flight calibration. A brief discussion about the potential application of Fasat-C is presented in Section 6. Finally, Section 7 summarizes this work.

2. Fasat-C overview

Fasat-C is the first high spatial resolution mission operated by the Chilean Air Force (FACH). The Fasat-C acquires 10-bit data in five spectral bands covering panchromatic (455–744 nm), blue (455–520 nm), green (528–588 nm), red (625–695 nm) and near-infrared (758–881 nm) wavelengths. At nadir, the nominal ground sample distance is 1.45 m (panchromatic band) and 5.8 m (multispectral bands) with a nominal swath width of 10 km.

The NAOMI-1 instrument on-board Fasat-C is a pushbroom imager, which constructs an image one row at a time as the focused image of the Earth through the telescope moves across the linear detector arrays on the focal plane. It has a heliosynchronous orbit at an altitude of 620 km with an inclination of 97.8°. The satellite has a revisit time of 3–5 days with a viewing angle between ±30°, and a 37 days revisit time with a nadir view angle. Table 1 summarizes the technical information of the Fasat-C.

The spectral response function of the NAOMI-1 instrument is a key element for ground calibration and spectral comparisons. The normalized spectral response curves for each of the Fasat-C bands are shown in Fig. 1.

Three level of Fasat-C product are available: Level 1A product, which presents the radiometrically corrected images; Level 2 product which includes the geometric correction and the Level 3 product in which a pan-sharpening MTF procedure (Modulation Transfer Function) is performed (SAF technical report, 2013). Finally, the Fasat-Charlie has stereo capability (forward/backward) that allows the generation of digital elevation models of high spatial resolution.

Table 1
Fasat-Charlie technical specifications.

Spectral bands	Bandwidth (nm)
Blue	455–520
Green	528–588
Red	625–695
Near-infrared (NIR)	758–881
Panchromatic	455–744
Orbital altitude (km)	620
Orbital inclination	97.8° Sun-synchronus
Orbital period	97 min
Revisit capability	37 days Nadir 3–5 days with tailting capability of roll ±30°
Swath width	10 km
Coverage capability per scene	10 × 10 km
Type sensor	Pushbroom imager
Data quantization (radiometric)	10 bit
Spatial resolution	5.8 m at Multispectral/1.45 m at panchromatic

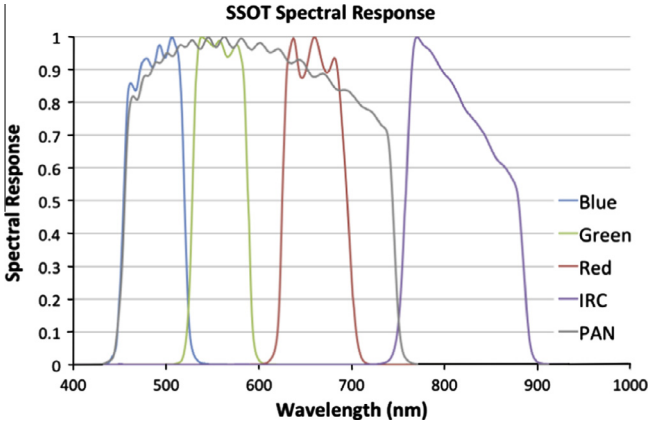

Fig. 1. Normalized spectral response for each Fasat-C spectral band.

3. Study area and data acquisition

3.1. Antumapu study area and ground measurements

Antumapu is one of University of Chile campuses, which is dedicated to Agricultural, Forest and Natural Renewable Resources sciences. It is located in the southern part of Santiago, Chile (33°33′59″S; 70°37′56″W). This area extends over more than 300 ha and is covered by crops, green grass and manmade surfaces. During the summer season (December–February), climate conditions are characterized by clear skies and dry atmosphere. Several annual crops are continuously harvested during the year at the Antumapu site. In order to make the field measurements, three covers with homogeneous spectral response over a year were selected for in situ calibration. These land covers are irrigated and managed green grass (soccer field), concrete and bare soil. The soccer field (100 × 75 m) was selected since this land cover type has been used in several field campaigns developed in the past. For instance, during the Dual-use European Security IR Experiment (DESIREX) 2008, a field campaign conducted over Madrid city, a green grass rugby field was used to calibrate and validate hyperspectral airborne images. Moreover, during the THERMOPOLIS 2009 field campaign carried out over Athens, the Panathinaikos soccer field (inside the city) was also used to calibrate and validate remote sensing images (Sobrino et al., 2009b, 2012a,b; Daglis et al., 2010a,b). Furthermore, a turf managed green grass was also used as calibration and validation target for SPOT imagery (Sandmier, 2000; Clark et al., 2011a,b). The concrete cover belongs to an outdoor hard court with dimensions of 30 × 50 m. Finally; the bare soil cover is still used as a parking lot which dimensions are 10 × 35 m. This land cover presents several clasts mixed with a loamy sand soil texture.

Ground measurements were carried out using an ASD spectroradiometer over these three land covers. The ASD (Analytical Spectral Devices) Handheld FieldSpec is a 512 element photodiode array spectroradiometer with a 325–1075 nm wavelength range, 1.5 nm sampling (bandwidth), 3.5 nm resolution and scan times as short as 17 ms. The calibration of the instrument was performed at the Geo Forschungs Zentrum (GFZ) and includes the wavelength calibration using a standard emission line lamp. In order to minimize the random error related to each measurement, the instrument was set to average ten measurements for each target scan. After one scan on the target cover, a reference scan of a calibrated Spectralon reference panel (Labsphere Inc.) was made. It is assumed that there is no significant variation of the atmospheric conditions between the target scan and the reference scan a few seconds later. Geographic coordinates (latitude and longitude) were registered for each target scan using a GPS system with a positioning error of around ±1 m. The numbers of points concerning the in situ measurements are detailed as follows: 17 points for green grass cover, 10 points for concrete cover and 6 points for the bare soil cover, which makes a total of 33 points with 10 averaged measurements for each scan. Each point is matched to its corresponding Fasat-C pixel in the L2 image. These in situ measurements were performed close to the Fasat-C overpass time (between 10:50 and 11:30 local time). That information, in addition to the technical description of the acquired Fasat-C images is described in the next section. Finally, Fig. 2 shows the study area, the land surface covers selected for measurement and the point sample distribution over the study area.

3.2. Fasat-C images

One Fasat-C Level 2 multispectral (5.8 m) and one panchromatic (1.45 m) image were used in this work. The acquisition of these images over the Antumapu site was carried on January 29th, 2013 at 10:56:21 local time (14:56:21 UTC time). Table 1 summarizes the geometric conditions of the Fasat-C imagery used in this work in addition to the Fasat-C spectral bands.

3.3. MODIS products

Atmospheric characterization is relevant for every image-processing task where surface physical variables are estimated (Karpouzli and Malthus, 2003). Thus, the characterization of aerosols, water vapor and ozone has a high importance for surface reflectance estimations. Because no spectral surface irradiance was measured at the time of Fasat-C's overpass, atmospheric products from the Moderate Resolution Imaging Spectroradiometer (MODIS) were used to characterize the atmospheric conditions. These products have been used in other scientific publications with reliable results and remarking the usefulness of MODIS atmospheric data for Atmospheric correction (Gillingham and Shepherd, 2004; Norjamäki and Tokola, 2007; Jiménez-Muñoz et al., 2010, 2014).

The MODIS products used in this work are described as follows: MODIS Atmospheric profile product (MOD04_L2) dataset (Kaufman and Tanré, 1998) was used to obtain the Aerosol Optical Depth (AOD) at 550 nm at a 10 × 10 km spatial resolution; ozone concentration was derived from the MOD07 dataset (Gao and

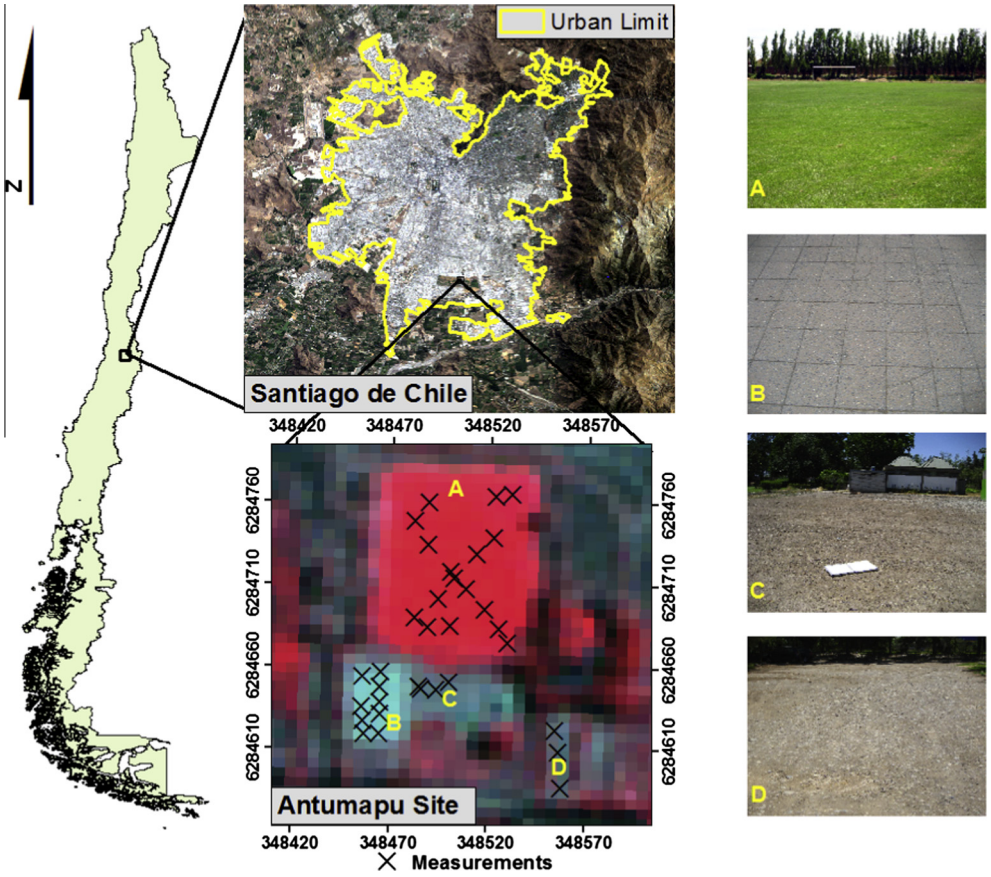

Fig. 2. Study area and pictures of green grass (A), concrete (B) and bare soil (C and D) land covers.

Kaufman, 1998) at a 5 × 5 km resolution and water vapor concentration at a 1 × 1 km resolution was derived from MOD05 data (Seemann et al., 2002).

3.4. Library spectra

Laboratory spectra measurements have been widely used as additional information in field campaigns and remote sensing calibration/validation processes (Sobrino et al., 2009a). In this work, the green grass spectra presented in the Aster Spectral Library (ASL) by Baldridge et al. (2009) was selected for spectra comparison with Fasat-C data and in situ spectra measurements. A detailed description of the spectra comparison is presented in Section 4.3.

4. Methods

4.1. Fasat-C radiometric calibration procedure

The radiometric calibration of Fasat-C consists in converting the Digital Number (DN) to at-sensor radiance and reflectance. The Digital Numbers (DN) of the Fasat-C images (multispectral and panchromatic) were converted to at-sensor radiance for each spectral band using (1):

$$L_\lambda = DN_\lambda \cdot (Gain_\lambda)^{-1} + Physical\ Bias \quad (1)$$

where λ is the Fasat-C spectral band, L_λ is the at-sensor apparent radiance (W m^{-2} μm^{-1} str^{-1}), DN_λ is the Digital Number of each band (0–1024), *Gain* is the conversion coefficients (0.9338110; 1.0134981; 1.2136321; 1.5855519 and 1.275168 for the blue, green, red, near-infrared and panchromatic channels respectively). The physical bias was considered to be equal to zero (SAF technical report, 2013). Gain coefficients were used as the default values to obtain the at-sensor radiance. The coefficients were obtained in laboratory conditions and had never been tested before for in-flight calibration over agricultural areas. Thus, the applications of a first calibration can allow to test the reliability of these coefficients and also to analyze the spectral variation including atmospheric correction. Once the Fasat-C images were converted to radiance, the at-sensor reflectance can be derived using (2):

$$\rho_\lambda = \frac{\pi \cdot L_\lambda \cdot d^2}{Esun_\lambda \cdot \cos(\theta)} \quad (2)$$

where ρ_λ is the spectral reflectance, d is the Earth–Sun distance in astronomic units (0.98496 for the 01/29/2013), π is a constant equal to 3.1415927, θ is the solar zenith angle given by the image acquisition time, and *Esun* (W m^{-2} μm^{-1}) is the mean solar irradiance at the top of the atmosphere for the λ band. This last parameter was estimated using the normalized spectral response of each Fasat-C band and the solar irradiance spectra proposed by Thuillier et al. (2003). Both spectra were convolved as shown in (3).

$$Esun_\lambda = \frac{\int_0^\infty Esun(\lambda) \cdot R'(\lambda) d\lambda}{\int_0^\infty R'(\lambda) d\lambda} \quad (3)$$

where $Esun(\lambda)$ is the solar spectrum published by Thuillier et al. (2003) and R'_λ is the spectral response of each spectral band. The Thuillier's solar spectrum is recommended by the Committee on Earth Observation Satellites (CEOS) Working Group on Calibration and Validation (WGCV) for being more accurate and an improvement over other solar spectrum models (Chander et al., 2009) such as the Rossow 1985 (Rossow et al., 1985); Wehrli 1985 (Wehrli, 1985); Kneizys 1988 (Kneizys et al., 1988) and ASTM E-490 (ASTM, 2000).

4.2. Atmospheric correction

The Second Simulation of a Satellite Signal in the Solar Spectrum (6S) radiative transfer code (Vermote et al., 1997) was used to estimate surface reflectance values from sensor measurements. The 6S model has been widely used for remote sensing atmospheric correction since this code is practical, fast and efficient. Several works have applied this method to correct airborne imagery (less than 3 m of spatial resolution) (Franch et al., 2013; Mattar et al., 2014), remote sensing imagery at high (less than 5 m) (Martin et al., 2012), medium (between 15–90 m) (Jiménez-Muñoz et al., 2010) and coarse spatial resolution (between 250–1000 m) (Vermote et al., 1997). In fact, one of the widely used surface reflectance products (MOD09) derived from MODIS data uses the atmospheric correction of the 6S model.

The atmospheric parameters for water vapor (W), ozone (O_3) and Aerosol Optical Depth (AOD) provided by the MODIS products were used as input values of the 6S model. Also, several values of W, O_3 and (AOD) were tested in order to analyze the atmospheric influences on the at-sensor radiance and therefore the effects over surface reflectance. Table 2 summarizes the initial concentrations for W, O_3 and AOD derived from MODIS products and the additional test values. A similar procedure concerning initial concentrations and additional parameters to test the reliability of the atmospheric correction was published in Jiménez-Muñoz et al. (2010) about the MODIS product used to correct Visible, Near-Infrared and Thermal imagery.

Table 2
Geometric corners, sun–satellite position and atmospheric data at the moment of imagery acquisition.

Geometric conditions	Values				
Upper left	W 70°39′43″S 33°28′33″				
Down left	W70°41′16″S33°34′04″				
Upper right	W 70°33′12″S33°29′47″				
Down right	W70°34′45″S33°35′17″				
Central position	W70°37′14″S33°31′54″				
Sun–satellite position	**Angles**				
Satellite incidence angle	5.76°				
Satellite azimuth angle	99.99°				
Sun azimuth angle	67.50°				
Sun elevation angle	59.36°				
Atmospheric conditions	**MODIS**	**Test values**			
Water content – Uw (g/cm^2)	1.639	0.5	1.0	2.0	3.0
Ozone content – U_{OZ} (cm-atm)	0.273	0.1	0.2	0.3	0.5
Aerosol Optical Depth at 550 nm	0.063	0.03	0.1	0.2	0.3
Aerosol type	Urban				

4.3. Ground comparison

The surface reflectance estimated from Fasat-C data was compared to the ground spectra measured for each surface cover. The comparison was carried out for the multispectral and panchromatic images. To obtain the mean reflectance for the Fasat-C spectral bands, the Relative Spectral Response Calculator (RSRc®) (Durán-Alarcón et al., 2014) was used. The RSRc® calculator is a free software currently available for scientific purposes which can convolve any spectrum for a given filtering function. This procedure was also carried out for the green grass spectra derived from the ASL to compare green grass measurements.

The comparison was performed for each of the three selected covers and for the whole set of measurements using the bias, standard deviation and root mean square error (RMSE). Finally, a statistical analysis consisting in a linear regression between surface reflectance derived from the Fasat-C and in situ measurements was made. Fig. 3 presents the flowchart of the aforementioned methodology.

5. Results

5.1. Esun values

The exoatmospheric irradiance for each Fasat-C spectral band is presented in Table 3. Thuillier et al. (2003) sun solar spectrum is considered as the standard by the CEOS community following the

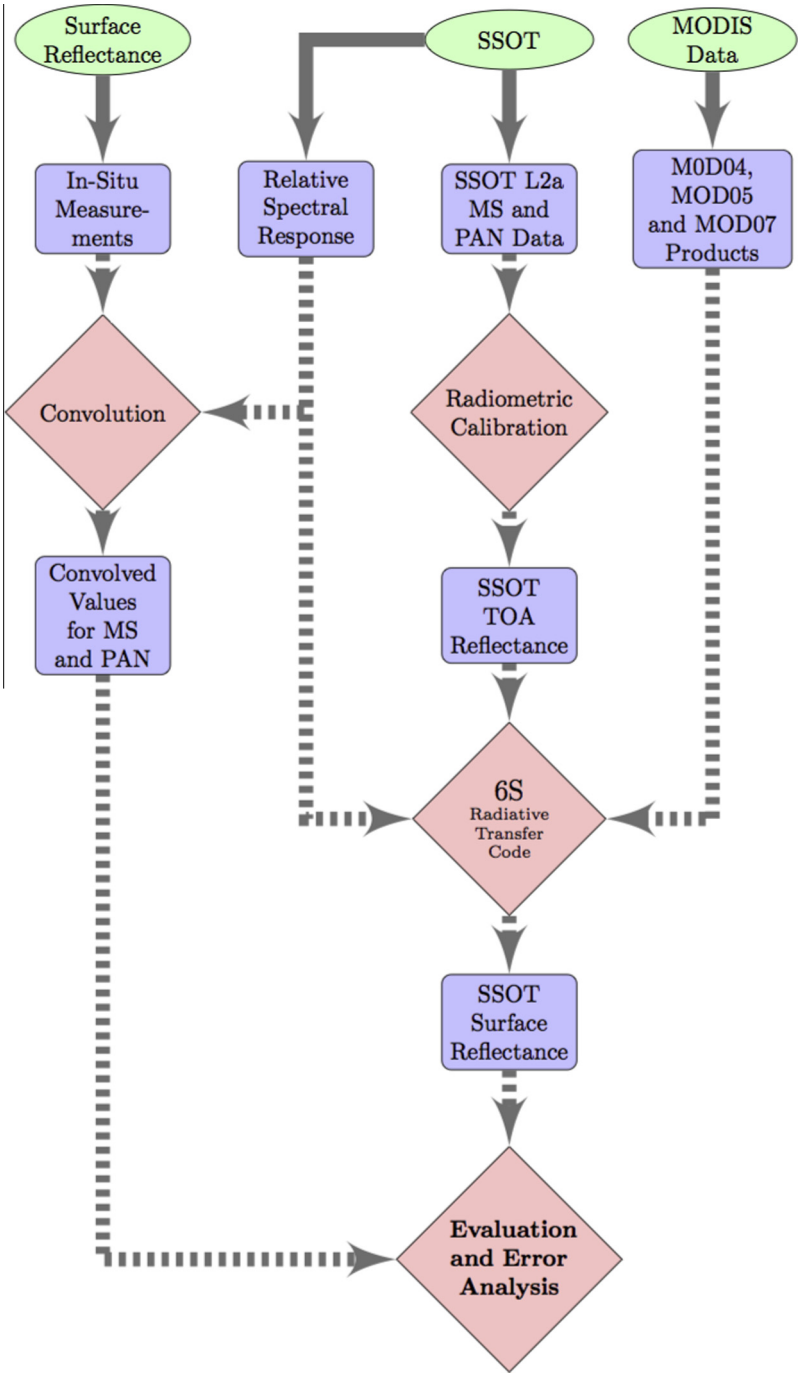

Fig. 3. Flowchart of the proposed methodology for the evaluation of multispectral (MS) and panchromatic (PAN) Fasat-C images.

Table 3
Mean exo-atmospheric irradiance estimated for each Fasat-C spectral band.

Fasat-C band	Solar spectrum source					% Error from Thuillier et al. (2003)			
	Thuillier et al. (2003)	ASTM (2000)	Kneizys et al. (1988)	Rossow et al. (1985)	Wehrli (1985)	ASTM (2000)	Kneizys et al. (1988)	Rossow et al. (1985)	Wehrli (1985)
Blue	1977.95	1949.71	1954.74	1954.49	1951.71	1.43	1.17	1.19	1.33
Green	1825.62	1851.95	1856.86	1855.53	1854.03	1.44	1.71	1.64	1.56
Red	1538.27	1553.83	1557.62	1556.38	1555.83	1.01	1.26	1.18	1.14
NIR	1091.43	1100.0	1103.19	1102.98	1101.42	0.79	1.08	1.06	0.92
Pan	1706.90	1714.01	1718.39	1717.81	1715.98	0.42	0.67	0.64	0.53

analysis presented in Chander et al. (2009). However, when using other solar spectra and convolving them using the Fasat-C relative spectral response, the exoatmospheric sun values for each multispectral and panchromatic band varied by between 1% and 2% (about 20 W m^{-2}). Some slight differences can be evidenced for the blue and green bands and the lowest differences were obtained for the NIR and the PAN channels. Neverthless, this variation is not statistically significant when the reflectance values are derived from the Fasat-C computed spectral radiance.

5.2. Surface reflectance comparison

Atmospherically corrected surface reflectance values were compared to in situ measurements through the calculation of the bias, σ and RMSE. For the green grass cover, the error values are lower than 2% for the blue, green, red and panchromatic bands. As expected, the NIR band presents the highest values of surface reflectance, although the bias and σ give this band the highest RMSE.

The green grass cover evidenced high amplitude in surface reflectance values at the moment of measurement not evidenced before. Fig. 4 shows the spatial variability of the surface reflectance achieved over the green grass cover. Three different areas can be distinguished on the NIR band: a central zone with lower values of green grass, a particular zone with higher values and the rest of the field. This effect can be attributed to two different factors, the green grass varieties present in the field that have grown and merged in the same area, and the field use for other activities. The green grass cover belongs to a soccer field, which presents an intensive daily irrigation and weekly use. So, the center of the

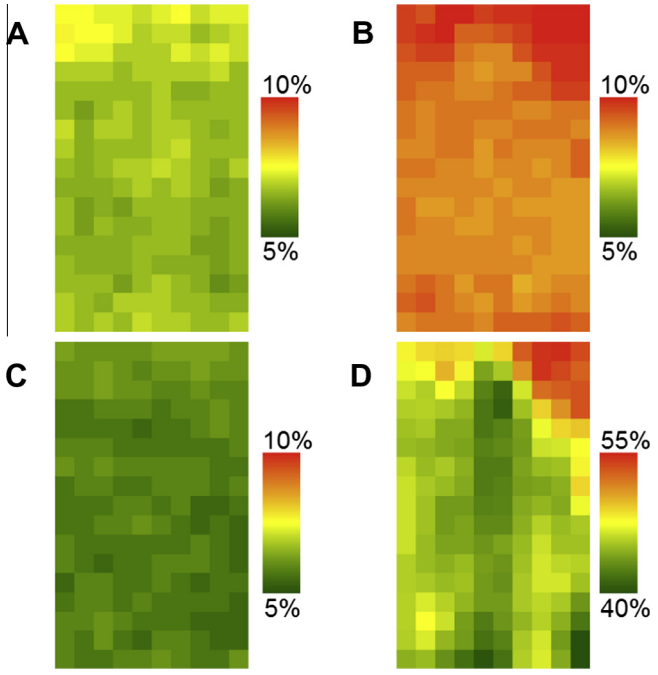

Fig. 4. Spatial variability of the surface spectral reflectance for blue (A), green (B), red (C) and near infrared (D) bands over green grass. (For interpretation of the references to color in this figure legend, the reader is referred to the web version of this article.)

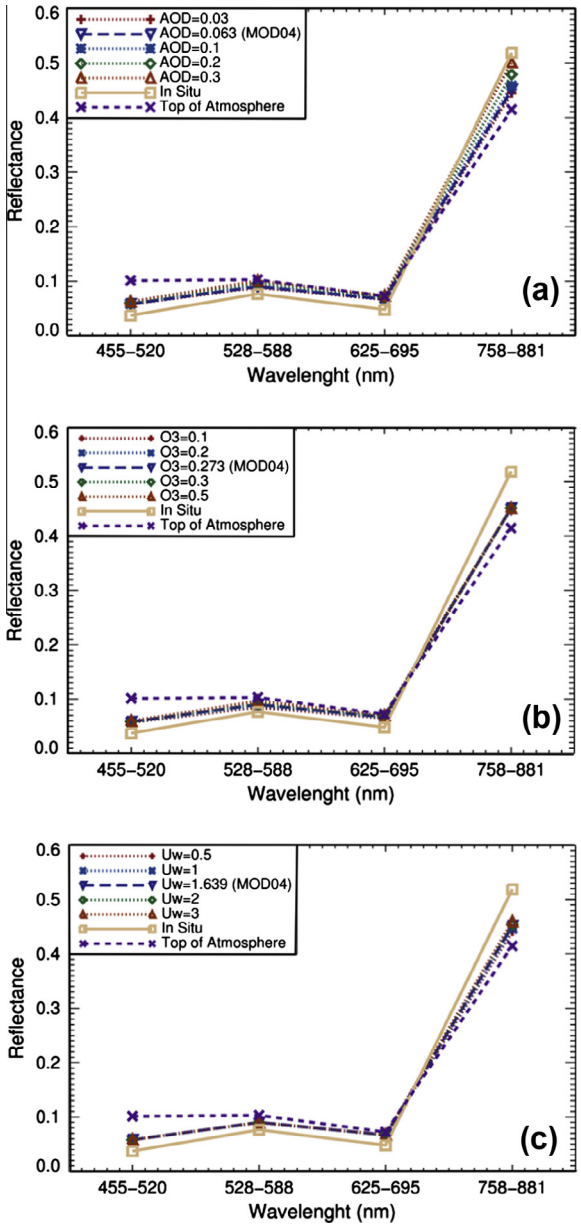

Fig. 5. Green grass reflectance estimated from ground measurements and Fasat-C data for blue (455–520 nm), green (528–588 nm), and red (625–695 nm) and near-infrared (758–881 nm). The test values of AOD (a), O_3 (b) and W (c) are also shown. The values derived from MODIS products are indicated in the legend.

green grass field tends to present less vegetation cover and also low values of surface reflectance in comparison with the borders. Moreover, the grass varieties planted were spatially uniform which also contributes to generate a heterogeneous surface. These factors have strongly influenced the green grass cover structure and therefore, the photosynthetic activity. Accounting for the green grass spectra from the ASL, the RMSE between in situ measurements and the ASL green grass spectra are 1.0%; 2.4%; 0.9% and 6.3% for blue, green, red and NIR bands respectively. These errors diminished when the surface reflectance estimated from each Fasat-C band is compared with the ASL convolved values for the green grass. Those RMSE are 1.1%; 1.0%; 1.2% and 4.2% for blue, green, red and NIR bands respectively.

The effect of the atmospheric correction on the green grass spectral signature can be seen in Fig. 5. The correction procedure over each other Fasat-C band presents a high/low effect on the NIR and blue band respectively. For the blue band, the surface reflectance values have diminished in relation to the TOA (Top Of Atmosphere) values. Otherwise, in the NIR, the surface reflectance values have increased in relation to the TOA values. These effects are accounted for by the aerosol band absorption process in this region of the spectrum. It seems in Fig. 5a that AOD values can improve the surface reflectance values when considering a higher value of AOD in comparison with MODIS product (> than 0.2). Nevertheless, this change in the value of AOD is not relevant for the other bands. For all the concentration of AOD, the TOA reflectance presents the higher difference at comparing to ASL and in situ, denoting the effects of atmospheric correction. For both Fig. 5b and c, the effect of O_3 and W values over the estimated surface reflectance is quite similar for all spectral bands. It is important to denote that the atmospheric influence is higher in the blue and near-infrared bands (5–10% of the surface reflectance value).

The results obtained for bare soil are presented in Fig. 6. The RMSE for the blue, green and the panchromatic bands are about

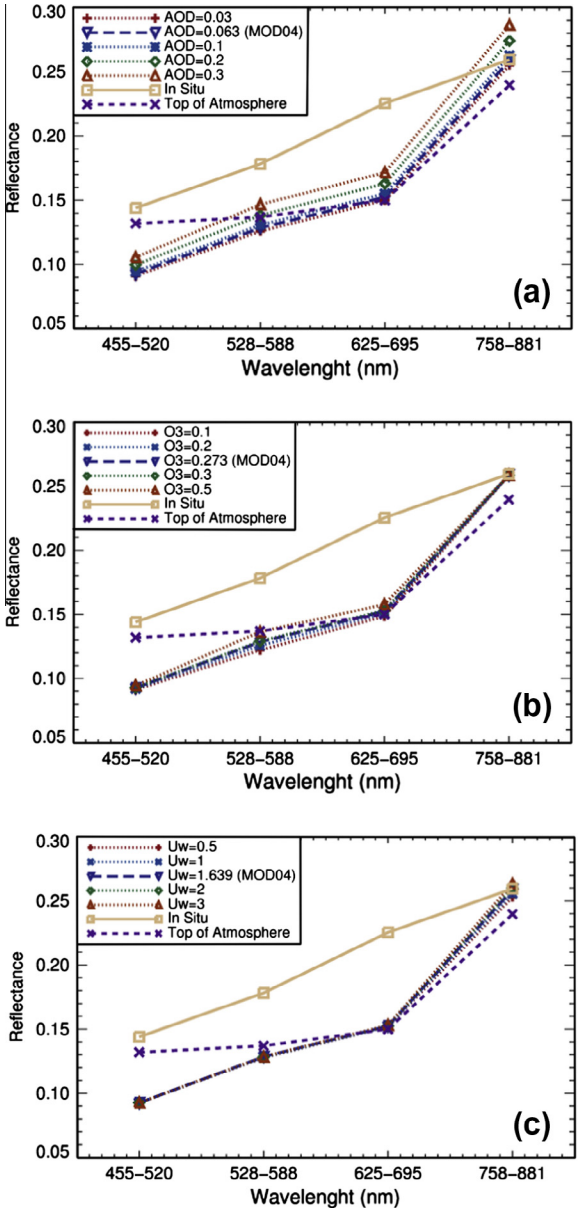

Fig. 6. Bare soil reflectance estimated from ground measurements and Fasat-C data for blue (455–520 nm), green (528–588 nm), and red (625–695 nm) and near-infrared (758–881 nm). The test values of AOD (a), O_3 (b) and W (c) are also shown. The values derived from MODIS products are indicated in the legend.

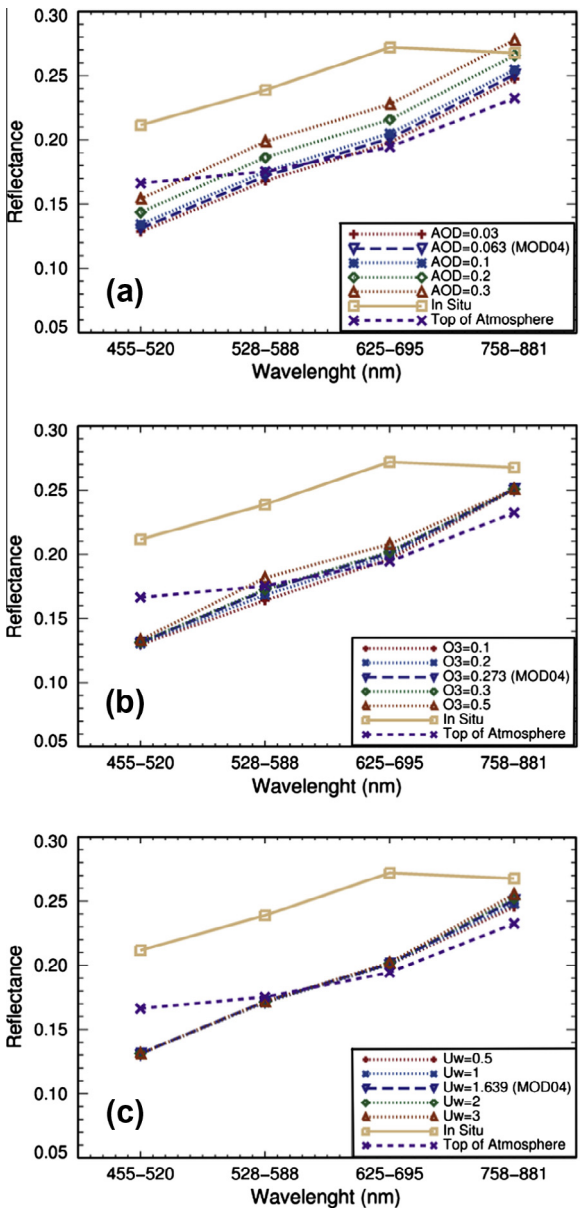

Fig. 7. Concrete reflectance estimated from ground measurements and Fasat-C data for blue (455–520 nm), green (528–588 nm), and red (625–695 nm) and near-infrared (758–881 nm). The test values of AOD (a), O_3 (b) and W (c) are also shown. The values derived from MODIS products are indicated in the legend.

Table 4
Surface reflectance comparison (%) between Fasat-Charlie and in situ measurements using MODIS atmospheric parameters in the atmospheric correction. Bias, σ and RMSE are presented.

Fasat-C band	Surface								
	Green grass			Bare soil			Concrete		
	Bias	σ	RMSE	Bias	σ	RMSE	Bias	σ	RMSE
Blue	−2.09	0.16	2.10	5.13	1.18%	5.27	8.03	1.38	8.15
Green	−1.36	0.49	1.44	4.97	1.26%	5.13	6.69	1.53	6.87
Red	−1.90	0.38	1.94	7.21	1.76%	7.50	7.07	1.58	7.25
NIR	6.74	3.86	7.76	0.08	1.40%	1.40	1.68	0.84	1.88
Pan	−8.56	0.67	8.59	−7.36	0.48	7.37	−4.34	5.2	6.77

5%, the red band presents a slightly higher RMSE value of ∼7%, and the near infrared band presents the lowest RMSE value of ∼2%. The bare soil cover is characterized mainly by stones, silicates particles and moist sand, so the influences on the surface reflectance are complex and difficult to characterize and compare. We did not evidence any significant difference between surface reflectance at using other values of AOD, O_3 or W for the bare soil cover. In the case of concrete (Fig. 7), the material composition (mainly silicates) is not homogeneous and the aggregated land path radiance could be systematically offset from the point-ground measurements obtained by the ASD. The maximum RMSE was evidenced for the blue band and the minimum for the near-infrared band. In general, the average RMSE or the concrete is about 5%. Similar results were obtained to the green grass cover where the higher values of AOD generate a lower RMSE (0.2–0.3 AOD). However, the at-sensor reflectance presents the highest value for the blue band probably attributed to some pigments contained in the concrete which has a peak in the blue band. For the different values of W and O_3, the influence on the atmospheric correction is less significant than that of the AOD.

Both bare soil and the concrete targets used in Antumapu test site can be considered as urban materials which are difficult to compare between ground and remote sensing imagery. Several papers have addressed the urban materials characterization by using a broad spectral library in the optical range (Herold et al., 2004; Baldridge et al., 2009), thermal range (Sobrino et al., 2012a,b) or synergic characterization by using reflectance and thermal data (Small, 2006; Roberts et al., 2012). The high degree of spatial and spectral heterogeneity of each targets (natural or artificial) require specific attention to the spectral dimension. In fact, the composition of the concrete can influence the surface spectral reflectance as is the case when comparing surface reflectance and the reflectance calculated at-sensor and at-surface from Fasat-C imagery.

6. Discussion

Considering both multispectral and panchromatic bands, a RMSE ranging between 1% and 10% was obtained over the three land covers considered in this work (Table 4). As a first in-flight calibration, the Fasat-C L2 product presents a reasonable performance when compared to ground measurements. Ground measurements were carried out on the Antumapu site which has shown several difficulties in its use as a remote sensing test site. Despite the fact that large homogeneous areas can be found in Antumapu, the spectral signature calculated for the covers used in this work are heterogeneous which influences the ground-sensor comparison. A dedicated well implemented agricultural or natural test site is desirable for further calibration/validation protocols. This site can be located in Chile or combined with an international site. For instance, the Barrax agriculture area which has been selected by the European Space Agency to carry out several field campaigns to test explorer satellite missions (Sobrino et al., 2008, 2009c, 2011)

For all the targets considered in this work (concrete, bare soil and green grass), the at-sensor reflectance for the blue band is slightly high and the atmospheric correction by using data from MODIS data is not enough to obtain reliable values of surface reflectance. Furthermore, MODIS products can be useful data for correcting the atmospheric effect in the optical range in spite of some bias that these data can introduce into spatial atmospheric correction. However, the atmospheric urban influences such as urban aerosols or other gases could not be accounted for in some areas because of MODIS products spatial resolution (larger than 1 km). Nevertheless, to correct Fasat-C imagery from the atmospheric effect by using the 6S radiative code and MODIS products a good performance considering its spatial resolution can be achieved for surface reflectance values. However, ground measurements have to be included in order to assess the radiative effects of correcting high spatial resolution imagery using coarse aerosol data. In this work, these effects are included in the ground–surface comparison between Fasat-C and in situ data. Given that Fasat-C multispectral bands were atmospherically corrected achieving low errors (∼3%), these results have to be tested in future works considering in situ atmospheric measurements.

The in situ atmospheric measurements are mandatory for further calibration over urban areas using Fasat-C imagery. In our case, the atmospheric contaminants and trace gases of Santiago influence the land leaving radiance captured by the Fasat-C for the scene analyzed in this work. The temporal and variablity of those atmospheric particles were anlayzed in several works (i.e. Didyk et al., 2000; Gramsch et al., 2006; Seguel et al., 2009; Muñoz and Alcafuz, 2012). Other efforts were conducted to analyze the relation between particulate matter concentration over Santiago and climatic oscilation (Ragsdale et al., 2013). However, a comprehensive spatial and temporal concentration analysis of these urban gases such as particulate matter and pollutants is still underway because of the scarce number of monitoring stations in addition to the topography and seasonal atmospheric patterns. All these factors generate a spatial gap in some areas of Santiago. This gap produced in southern part of Santiago is poorly described by MODIS products and therefore the surface reflectance obtained from the 6S corrections can be over or under estimated. A possible way to improve the atmospheric corrections over Santiago is based on the use of Lidar measurements performed in the northwest part of the city (Muñoz and Alcafuz, 2012). Neverthless, these atmospheric measurements need to be accompained by in situ surface reflectance values registered for several targets located near the LIDAR location.

7. Conclusion

In this work a Fasat-C Level 2 image was used for the first in-flight calibration which was carried out over Antumapu site located in Santiago de Chile. Because it is in urban area, aerosol influences are hard to correct without in situ profiles. Despite the fact that MODIS products could be considered useful for

atmoshperic correction, error is introduced because of the spatial resolution of the MODIS aerosol, water vapor and ozone products. Further calibration/validation procedures will be carried out in order to test the realiability of Fasat-C images over diverse land surface covers in addition to investigating the other potential capabilities such as the stereo images and the pansharpening processing method.

The conversion from Digital Number to at-sensor reflectance in addition to the exoatmospheric values have been also described. By comparing the at-surface reflectance derived from Fasat-C with in situ ground measurements, the relative error for the multispectral band is about 5%, additionally, the panchromatic comparison showed a similar error for the green grass, concrete and bare soil covers. The blue band may present an overestimation which invites to recalibrate the original gain coefficients. Further cross calibration/validation field campaigns will be carried out in order to analyze possible improvements that could be done to the spectral comparison on the multispectral and panchromatic values.

Acknowledgments

This work was partially funded by Program U-INICIA VID 2012, grant U-INICIA 4/0612; University of Chile, Santander– University of Chile grant for young scientist and Fondecyt-Initial (CONICYT/ref-11130359). The authors also thank the MODIS team for providing atmospheric products (http://modis-atmos.gsfc.nasa.gov/) and Dr. L. Morales for the reference panel provided to obtain in situ measurements.

References

ASTM-2000, 2000. ASTM E490 Solar Constant and Zero Air Mass Solar Spectral Irradiance Tables. ASTM, West Conehohocken, US, pp. 1–16.

Baldridge, A.M., Hook, S.J., Grove, C.I., Rivera, G., 2009. The ASTER spectral library version 2.0. Remote Sens. Environ. 113, 711–715.

Chander, G., Markham, B.L., Helder, D.L., 2009. Summary of current radiometric calibration coefficients for Landsat MSS, TM, ETM+, and EO-1 ALI sensors. Remote Sens. Environ. 113, 893–903.

Clark, B., Suomalainen, J., Pellikka, P., 2011a. An historical empirical line method for the retrieval of surface reflectance factor from multi-temporal SPOT HRV, HRVIR and HRG multispectral satellite imagery. Int. J. Appl. Earth Obs. Geoinf. 13 (2), 292–307.

Clark, B., Suomalainen, J., Pellikka, P., 2011b. The selection of appropiate spectrally bright pseudo-invariant ground targets for use in empirical line calibration of SPOT satellite imagery. ISPRS J. Photogramm. Remote Sens. 66 (4), 429–445.

Daglis, I.A., Keramitsoglou, I., Amiridis, V., Petropoulos, G., Melas, D., Giannaros, T., Kourtidis, K., Sobrino, J.A., Manunta, P., Gröbner, J., Paganini, M., Bianchi, R., 2010. Investigating the urban heat island (UHI) effect in Athens through a combination of space, airborne and ground-based observations. In: Proceedings of COMECAP 2010 (Conference on Meteorology, Climatology and Atmospheric Physics 2010), University of Patras, 2010.

Daglis, I.A., Rapsomanikis, S., Kourtidis, K., Melas, D., Papayannis, A., Keramitsoglou, I., Giannaros, T., Amiridis, V., Petropoulos, G., Georgoulias, A., Sobrino, J.A., Manunta, P., Gröbner, J., Paganini, M., Bianchi, R., 2010. Results of the DUE THERMOPOLIS campaign with regards to the urban heat island (UHI) effect in Athens. In: ESA SP-686 Proceedings of the ESA Living Planet Symposium 2010, European Space Agency.

Didyk, B.M., Simoneit, B.R.T., Pezoa, L.A., Riveros, M.L., Flores, A.A., 2000. Urban aerosol particles of Santiago, Chile: organic content and molecular characterization. Atmos. Environ. 34 (8), 1167–1179.

Durán-Alarcón, C., Santamaría-Artigas, A., Valenzuela, N., Mattar, C., 2014. El RSR calculator, una herramienta útil para el proceso de calibración/validación. Aplicación al sensor Landsat 8 (LDCM). Revista de Teledetección.

Franch, B., Vermote, E.F., Sobrino, J.A., Fédèle, E., 2013. Analysis of directional effects on atmospheric correction. Remote Sens. Environ. 128, 276–288.

Gao, B., Kaufman, Y., 1998. The MODIS Near-IR Water Vapor Algorithm – Algorithm Theoretical Basis Document. MOD05.

Gillingham, S.S., Shepherd, J.D., 2004. Evaluation of MODIS for atmospheric correction of landsat ETM+ imagery. J. Spatial Sci. 49 (2), 43–56.

Gramsch, E., Cereceda-Balic, F., Oyola, P., von Baer, D., 2006. Examination of pollution trends in Santiago de Chile with cluster analysis of PM10 and ozone data. Atmos. Environ. 40 (28), 5464–5475.

Herold, M., Roberts, D., Gardner, M., Dennison, P., 2004. Spectrometry for urban area remote sensing—development and analysis of a spectral library from 350 to 2400 nm. Remote Sens. Environ. 91, 304–319.

Jiménez-Muñoz, J.C., Sobrino, J.A., Mattar, C., Franch, B., 2010. Atmospheric correction of optical imagery from MODIS and reanalysis atmospheric products. Remote Sens. Environ. 114, 2195–2210.

Jiménez-Muñoz, J.C., Sobrino, J.A., Mattar, C., Hulley, G., 2014. Temperature and emissivity separation from MSG/SEVIRI data. IEEE Trans. Geosci. Remote Sens. http://dx.doi.org/10.1109/TGRS.2013.2293791.

Karpouzli, E., Malthus, T., 2003. The empirical line method for the atmospheric correction of IKONOS imagery. Int. J. Remote Sens. 24 (5), 1143–1150.

Kaufman, Y.J., Tanré, D., 1998. Algorithm for Remote Sensing of Troposhperic Aerosol from MODIS.

Kneizys, F.X., Shettle, E.P., Abreu, L.W., Chetwynd, J.H., Anderson, G.P., Gallery, W.O., Selby, J.E.A., Clough, S.A., 1988. Users Guide to LOWTRAN 7. AFGL-TR-0177, Environmental Research Papers, 1010.

Martin, J., Eugenio, F., Marcello, J., Medina, A., Bermejo, J.A., Arbelo, M., 2012. Atmospheric correction models for high resolution WorldView-2 multispectral imagery: a case study in Canary Islands, Spain. In: Remote Sensing of Clouds and the Atmosphere XVII; and Lidar Technologies, Techniques, and Measurements for Atmospheric Remote Sensing VIII. Proceedings of the SPIE, 8534, p. 10.

Mattar, C., Franch, B., Sobrino, J.A., Corbari, C., Jiménez-Muñoz, J.C., Olivera-Guerra, L., Skokovic, D., Soria, G., Oltra-Carrio, R., Julien, Y., Mancini, M., 2014. Impacts of the broadband albedo on actual evapotranspiration estimated by S-SEBI model over an agricultural area. Remote Sens. Environ. 147, 23–42.

Muñoz, R., Alcafuz, R., 2012. Variability of Urban aerosols over Santiago, Chile: comparison of surface PM10 concentrations and remote sensing with Ceilometer and Lidar. Aerosol Air Qual. Res. 12, 8–9.

Norjamäki, I., Tokola, T., 2007. Comparision of atmoshperic correction methods in mapping timber volume with multitemporal landsat images in Kainuu, Finland. Photogramm. Eng. Remote Sens. 73 (2), 155–163.

Ragsdale, K.M., Barret, B.S., Testino, A.P., 2013. Variability of particulate matter (PM10) in Santiago, Chile by phase of the Madden–Julian Oscillation (MJO). Atmos. Environ. 81, 304–310.

Roberts, D., Quattrochi, D., Hulley, G., Hook, S., Green, R., 2012. Synergies between VSWIR and TIR data for the urban environment: an evaluation of the potential for the Hyperspectral Infrared Imager (HyspIRI) decadal survey mission. Remote Sens. Environ. 117, 83–101.

Rossow, W.B., Kinsella, E., Wolf, A., Gardner, L., 1985. Description of Reduced Resolution Radiance Data. WCRP/ISCCP, WMO/TD No. 58.

Roy, D., Borak, J., Devadiga, S., Wolfe, R., Zheng, M., Descoiters, J., 2002. The MODIS land product quality assessment approach. Remote Sens. Environ. 83, 62–76.

SAF (Servicio Aéreo Fotogramétrico de Chile), 2013. SSOT Technical Report. Available on: <http://www.saf.cl/images/Material%20PDF/FASAT-C_Specs_v1.4.pdf>.

Sandmier, S., 2000. Acquisition of bidirectional reflectance factor data with field goniometers. Remote Sens. Environ. 73, 257–269.

Seemann, S.W., Borbas, E.E., Li, J., Menzel, W.P., Gumley, L.E., 2002. Modis Atmospheric Profile Retrieval Algorithm Theoretical Basis Document. MOD07.

Seguel, R., Morales, R.G., Leiva, M.A., 2009. Estimations of primary and secondary organic carbon formation in PM2.5 aerosols of Santiago City, Chile. Atmos. Environ. 43 (13), 2125–2131.

Small, C., 2006. Comparative analysis of urban reflectance and surface temperature. Remote Sens. Environ. 104 (2), 168–189.

Sobrino, J.A., Jimenez-Muñoz, J.C., Soria, G., Gomez, M., Barella Ortiz, A., Romaguera, M., Zaragoza, M., Julien, Y., Cuenca, J., Atitar, M., Hidalgo, V., Franch, B., Mattar, C., Ruescas, A., Morales, L., Gillespie, A., Balick, L., Su, Z., Nerry, F., Peres, L., Libonati, R., 2008. Thermal remote sensing in the framework of the sen2flex project: field measurements, airborne data and applications. Int. J. Remote Sens. 29 (17–18), 4961–4991.

Sobrino, J.A., Mattar, C., Pardo, P., Jiménez-Muñoz, J.C., Hook, S.J., Barldridge, A., Ibañez, P., 2009a. Soil emissivity and reflectance spectra measurements. Appl. Opt. 48 (19), 3664–3670.

Sobrino, J.A., Sòria, G., Oltra-Carrió, R., Jiménez-Muñoz, J.C., Romaguera, M., Cuenca, J., Hidalgo, V., Franch, B., Mattar, C., Julien, Y., Bianchi, R., Paganini, M., Moreno, J.F., Alonso, L., Fernández-Renau, A., Gómez, J.A., de Miguel, E., Gutiérrez, Ó., Jiménez, M., Prado, E., Rodríguez-Cantano, R., Ruiz, I., Nerry, F., Najjar, G., Kastendeutch, P., Pujadas, M., Molero, F., Martilli, A., Salamanca, F., Fernández, F., Galán, E., Cañada, R., Hernández, E., Hidalgo, J., Acero, J.Á., Romero, J.M., Moya, F., Gimeno, L., 2009b. DESIREX 2008: estudio de la isla de calor en la ciudad de Madrid. Revista de Teledetección 31, 80–92.

Sobrino, J.A., Jiménez-Muñoz, J.C., Zarco-Tejada, P.J., Sepulcre-Cantó, G., de Miguel, E., Sória, G., Romaguera, M., Julien, Y., Cuenca, J., Hidalgo, V., Franch, B., Mattar, C., Morales, L., Gillespie, A., Sabol, D., Balick, L., Su, Z., Jia, L., Gieske, A., Timmermans, W., Olioso, A., Nerry, F., Guanter, L., Moreno, J., Shen, Q., 2009c. Thermal remote sensing from airborne hyperspectral scanner data in the framework of the sparc and sen2flex projects: an overview. Hydrol. Earth Syst. Sci. 13, 2031–2037.

Sobrino, J.A., Mattar, C., Gastellu-Etchegorry, J.P., Jiménez-Muñoz, J.C., Grau, E., 2011. Evaluation of DART 3D model in the thermal domain using satellite/airborne imagery and ground-based measurements. Int. J. Remote Sens. 32 (22), 7453–7477.

Sobrino, J.A., Oltra-Carrió, R., Soria, G., Bianchi, R., Paganini, M., 2012a. Impact of spatial resolution and satellite overpass time on evaluation of the surface urban heat island effects. Remote Sens. Environ. 117, 50–56.

Sobrino, J.A., Oltra-Carrió, R., Jiménez-Muñoz, J.C., Julien, Y., Soria, G., Franch, B., Mattar, C., 2012b. Emissivity mapping over urban areas using a classification-based approach: application to the Dual-use European Security IR Experiment (DESIREX). Int. J. Appl. Earth Obs. Geoinf. 18, 141–147.

Thome, K.J., Helder, D.L., Aaron, D., Dewald, J.D., 2004. Landsat-5 TM and Landsat-7 ETM+ absolute radiometric calibration using the reflectance-based method. IEEE Trans. Geosci. Remote Sens. 42, 2777–2785.

Thuillier, G., Herse, M., Labs, S., Foujols, T., Peetermans, W., Gillotay, D., Simon, P.C., Mandel, H., 2003. The solar spectral irradiance from 200 to 2400 nm as measured by SOLSPEC spectrometer from the ATLAS 123 and EURECA missions. Sol. Phys. 214 (1), 1–22.

Vermote, E., Tanré, D., Deuzé, J.L., Herman, M., Morcrette, J.J., 1997. Second simulation of the satellite signal in solar spectrum: an overview. IEEE Trans. Geosci. Remote Sens. 35, 675–686.

Wehrli, C., 1985. Extraterrestrial Solar Spectrum. WRC Pub. 615.